

# Time-reversal symmetry breaking in Re-based superconductors: Recent developments

T. Shang<sup>1,2,\*</sup> and T. Shiroka<sup>3,4,†</sup>

<sup>1</sup>Key Laboratory of Polar Materials and Devices (MOE), School of Physics and Electronic Science, East China Normal University, Shanghai 200241, China

<sup>2</sup>Laboratory for Multiscale Materials Experiments, Paul Scherrer Institut, Villigen CH-5232, Switzerland

<sup>3</sup>Laboratory for Muon-Spin Spectroscopy, Paul Scherrer Institut, Villigen PSI, Switzerland

<sup>4</sup>Laboratorium für Festkörperphysik, ETH Zürich, CH-8093 Zürich, Switzerland

In the recent search for unconventional- and topological superconductivity, noncentrosymmetric superconductors (NCSCs) rank among the most promising candidate materials. Surprisingly, some of them — especially those containing rhenium — seem to exhibit also time-reversal symmetry (TRS) breaking in their superconducting state, while TRS is preserved in many other isostructural NCSCs. To date, a satisfactory explanation for such discrepant behavior, albeit crucial for understanding the unconventional superconductivity of these materials, is still missing. Here we review the most recent developments regarding the Re-based class, where the muon-spin relaxation ( $\mu$ SR) technique plays a key role due to its high sensitivity to the weak internal fields associated with the TRS breaking phenomenon. We discuss different cases of Re-containing superconductors, comprising both centrosymmetric- and noncentrosymmetric crystal structures and ranging from pure rhenium, to  $\text{Re}T$  ( $T = 3d\text{-}5d$  early transition metals), to the dilute-Re case of  $\text{ReBe}_{22}$ .  $\mu$ SR results suggest that the rhenium presence and its amount are two key factors for the appearance and the extent of TRS breaking in Re-based superconductors. Besides summarizing the existing findings, we also put forward future research ideas regarding the exciting field of materials showing TRS breaking.

## I. INTRODUCTION

The combination of intriguing fundamental physics with far-reaching potential applications has made unconventional superconductors one of the most studied classes of materials. Standing out among them are the noncentrosymmetric superconductors (NCSCs) [1], whose crystal structures lack an inversion symmetry. As a consequence, in NCSCs, the strict symmetry-imposed requirements are relaxed, allowing mixtures of spin-singlet and spin-triplet Copper pairing channels, thus setting the scene for a variety of exotic properties, as e.g., upper critical fields beyond the Pauli limit, nodes in the superconducting gaps, etc. (see Refs. [1–3] for an overview). The degree of mixing in such combined pairings is related to the strength of the antisymmetric spin-orbit coupling (ASOC) and to other microscopic parameters, still under investigation. Currently, NCSCs rank among the foremost categories of superconducting materials in which to look for topological superconductivity (SC) or to realize the Majorana fermions, pairs of the latter potentially acting as noise-resilient qubits in quantum computing [4–11].

In general, the various types of NCSCs can be classified into two classes. One consists of strongly correlated materials, as e.g.,  $\text{CePt}_3\text{Si}$  [12], or  $\text{Ce}(\text{Rh},\text{Ir})\text{Si}_3$  [13], which belong to the heavy-fermion compounds. Owing to the strong correlation and the interplay between  $d$ - and  $f$ -electrons, these materials often exhibit rich magnetic and superconducting properties. Since their superconductivity is most likely mediated by spin fluctuations, this implies an unconventional (i.e., non phonon-related) pairing mechanism. Conversely, the other class consists mainly of weakly correlated materials, which are free of “magnetic”  $f$ -electrons, as e.g.,  $\text{LaNiC}_2$ ,  $\text{La}_7\text{Ir}_3$ ,  $\text{CaPtAs}$ , or  $\text{Re}T$  ( $T = 3d\text{-}5d$  early transition metals) [14–20]. Obviously, their superconductivity is not mediated by electrons’ spin fluctuations. Hence, they lend themselves as prototype parent systems where one can study the intrinsic pairing mechanisms in NCSCs.

Recently, superconductivity with broken time-reversal symmetry (TRS) has become a hot topic in NCSCs. The main reason for this is the discovery of TRS breaking in some weakly-correlated NCSCs using muon-spin relaxation ( $\mu$ SR). Surprisingly, the superconducting properties of the latter largely resemble those of conventional superconductors, i.e., they are clearly distinct from those of the above mentioned strongly-correlated NCSCs. To date, only a handful of NCSC families have been shown to exhibit TRS breaking in the superconducting state, including  $\text{LaNiC}_2$  [14],  $\text{La}_7(\text{Rh},\text{Ir})_3$  [15, 21],  $\text{Zr}_3\text{Ir}$  [22],  $\text{CaPtAs}$  [16], and  $\text{Re}T$  [14–20]. Except for the recently studied  $\text{CaPtAs}$ , where coexisting TRS breaking and superconducting gap nodes were observed below  $T_c$ , in most of the above cases the superconducting properties evidence a conventional  $s$ -wave pairing, characterized by a fully opened superconducting gap. This leads to an interesting fundamental question: does the observed TRS breaking in NCSCs originate from an unconventional superconducting mechanism (i.e., from a pairing other than that mediated by phonons), or it can occur also in presence of conventional pairing (via some not yet understood mechanism) [2, 3]? Why, among the many different NCSC families, only a few exhibit a broken TRS in the superconducting state, also remains an intriguing open question.

In general, the causes behind the TRS breaking at the onset of superconductivity are mostly unknown. In particular, the  $\alpha$ -Mn-type noncentrosymmetric  $\text{Re}T$  ( $T = \text{Ti}, \text{Nb}, \text{Zr}, \text{and Hf}$ ) superconductors have been widely studied and demonstrated to show a superconducting state with broken TRS [17–20]. Yet, TRS seems to be preserved in the isostructural (but Re-free)  $\text{Mg}_{10}\text{Ir}_{19}\text{B}_{16}$  and  $\text{Nb}_{0.5}\text{Os}_{0.5}$  [23, 24]. Further, depending on synthesis protocol,  $\text{Re}_3\text{W}$  is either a centro- (hcp-Mg-type) or a noncentrosymmetric ( $\alpha$ -Mn-type) superconductor, yet neither is found to break TRS [25]. In case of binary Re-Mo alloys, depending on the Re/Mo ratio, the compounds can exhibit up to four different crystal structures, including both centrosymmetric and noncentrosymmetric cases. Most importantly, all these alloys become superconductors at low temperatures [26]. A comparative  $\mu$ SR study of Re-Mo alloys, covering all the different crystal structures, reveals that the spontaneous magnetic fields occurring below  $T_c$  (an indication of TRS breaking) were

\* Corresponding authors:  
tshang@phy.ecnu.edu.cn

† Corresponding authors:  
tshiroka@phys.ethz.ch

only observed in elementary rhenium and in  $\text{Re}_{0.88}\text{Mo}_{0.12}$ . By contrast, TRS was preserved in the Re-Mo alloys with a lower Re-content (below  $\sim 88\%$ ), independent of their centro- or noncentrosymmetric crystal structures [27]. Since both pure rhenium and  $\text{Re}_{0.88}\text{Mo}_{0.12}$  have a simple (hcp-Mg-type) centrosymmetric structure, this strongly suggests that a noncentrosymmetric structure and the accompanying ASOC effects are not essential in realizing the TRS breaking in ReT superconductors. The  $\mu\text{SR}$  results regarding the Re-Mo family, as well as other Re-free  $\alpha$ -Mn-type superconductors, clearly imply that not only the Re presence, but also its amount are crucial for the appearance and the extent of TRS breaking in the ReT superconductors. How these results can be understood within a more general framework requires further experimental and theoretical investigations.

This short review article focuses mostly on the experimental study of Re-based binary superconductors. In Sec. II, we discuss the basic principles of our probe of choice, the  $\mu\text{SR}$ , here used to detect TRS breaking and to characterize the superconducting properties. Section III describes the possible crystal structures and superconducting transition temperatures of ReT binary alloys. In Sec. IV, we focus on the upper critical fields and the order parameter in ReT superconductors. Section V discusses the TRS breaking in ReT superconductors and its possible origins. Finally, in the last section, we outline some possible future research directions.

## II. MUON-SPIN RELAXATION AND ROTATION

Initially considered as an “exotic” technique, over the years muon-spin rotation, relaxation, and resonance (known as  $\mu\text{SR}$ ), has become one of the most powerful methods to study the magnetic and superconducting properties of matter. This follows from a series of fortunate circumstances, related to the muon properties as a fundamental particle. Most notably, these include the 100% initial muon-spin polarization, following the two-body decay from pions, and the subsequent preservation of such information through the weak decay into positrons. In the search for unconventional superconductivity, as well as for TRS breaking effects, the very high sensitivity of the  $\mu\text{SR}$  technique to tiny magnetic fields is especially important [28]. Below we briefly outline the basics of the  $\mu\text{SR}$  technique and direct the reader to other references for more detailed information [29–31].

### A. Principles of the $\mu\text{SR}$ technique

Central to the  $\mu\text{SR}$  method is the availability of polarized positive muon ( $\mu^+$ ) beams, obtained by collecting the muons produced in the two-body decay of positive pions,  $\pi^+ \rightarrow \mu^+ + \nu_\mu$  (with  $\nu_\mu$  the muon neutrino), decaying at rest in the laboratory frame. Since pions have no intrinsic angular momentum and neutrinos have a fixed helicity (relative orientation of spin and linear momentum), the resulting muon beam is 100% spin polarized, with the muon spins directed antiparallel to the linear momentum (see Figure 1A). Having an energy of  $\sim 4.12$  MeV, muons can penetrate a sample between 0.1 mm and 1 mm, depending on the sample density. Once implanted, the monoenergetic muons decelerate within 100 ps through ionization processes (which do not interact with the muon spin) and finally come to rest

at an interstitial site, practically without loss of their initial spin polarization. From this moment, if subject to magnetic interactions, the muon-spin polarization  $\mathbf{P}(t)$  evolves with time (the muon spin precesses around the local magnetic field), thus providing important information on the sample’s magnetism. The detection of the  $\mathbf{P}(t)$  evolution is made possible by the parity-violating weak-decay interaction  $\mu^+ \rightarrow e^+ + \nu_e + \bar{\nu}_\mu$  ( $e^+$ ,  $\nu_e$ , and  $\bar{\nu}_\mu$  are the positron, electron neutrino, and muon antineutrino, respectively), which implies a preferential emission of positrons along the muon-spin direction at the time of decay (see Figure 1A, which depicts also the anisotropic positron-emission pattern). Thus, by detecting the spatial distribution of positrons as a function of time, one can determine the time evolution of the muon-spin polarization  $\mathbf{P}(t)$ .

A schematic diagram of a time-differential  $\mu\text{SR}$  experiment is shown in Figure 1A. The incoming muon triggers a clock that defines the starting time  $t_0$ . Once implanted, the muon spin precesses about the local magnetic field  $\mathbf{B}(r)$  with a Larmor frequency  $\omega_\mu = \gamma_\mu B(r)$ , where  $\gamma_\mu/2\pi = 135.53$  MHz/T is the muon gyromagnetic ratio. The clock stops when, after a mean lifetime of 2.197  $\mu\text{s}$ , the muon decays into a positron  $e^+$ , registered as an event by one of the positron detectors. The measured time intervals for ca. 10–50 millions of such events are stored in a histogram, given by (see Figure 1B):

$$N(t) = N_0 \exp(-t/\tau_\mu) [1 + A_0 P(t)] + C. \quad (1)$$

Here, the exponential factor accounts for the radioactive muon decay,  $N_0$  is the initial count rate at time  $t_0$ , while  $C$  is a time-independent background (due to uncorrelated start and stop counts). As shown in the inset of Figure 1B, unlike the inessential exponential decay, the physical information in a  $\mu\text{SR}$  experiment is contained in the  $A(t) = A_0 P(t)$  term (often known as the  $\mu\text{SR}$  spectrum). Here,  $A_0$  is the so-called initial asymmetry (typically 0.3, depending on the detector’s solid angle and efficiency), while  $P(t)$  is the muon-spin depolarization function, here given by the projection of  $\mathbf{P}(t)$  on the unit vector describing the detector. Since  $P(t)$  represents the autocorrelation function of the muon spin  $\mathbf{S}$ , i.e.,  $P(t) = \langle \mathbf{S}(t)\mathbf{S}(0) \rangle / S(0)^2$ , it depends on the average value, the distribution, and the time evolution of the internal magnetic fields, thus reflecting the physics of the magnetic interactions in the sample under study. To access the  $\mu\text{SR}$  signal we need to remove the extrinsic decay factor by combining the positron counts from pairs of opposite-lying detectors, for instance,  $N_F$  and  $N_B$  (for forward and backward), and obtain the asymmetry  $A(t) = [N_F(t) - \alpha N_B(t)] / [N_F(t) + \alpha N_B(t)]$ . Clearly,  $A(t)$  behaves as a normalized detector “contrast”, proportional to  $A_0$ . The parameter  $\alpha$  is introduced to take into account the different efficiencies of the positron-detectors and needs to be determined by calibration.

### B. Transverse-field $\mu\text{SR}$

Depending on the reciprocal orientation of the external magnetic field  $\mathbf{B}$  with respect to the initial muon-spin direction  $\mathbf{S}(0)$ , in a  $\mu\text{SR}$  experiment, two different configurations are possible. (i) In transverse-field (TF)  $\mu\text{SR}$  the externally applied field  $\mathbf{B}$  is perpendicular to  $\mathbf{S}(0)$  and the muon spin

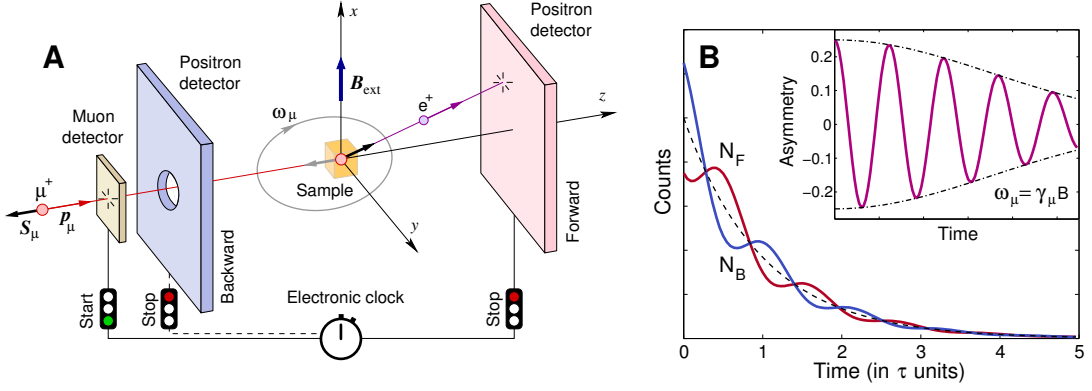


FIG. 1. Principle of the time-differential  $\mu$ SR experiment. (A) An incoming polarized muon (with spin  $S_\mu$  antiparallel to momentum  $p_\mu$ ) is first detected by a (thin) muon detector, which starts the electronic clock. In the sample, the muon spin precesses in the internal/external field until the muon decays into a positron. This is emitted preferentially along the muon-spin direction and hits one of the positron detectors [here forward (F) or backward (B)], whose signal stops the clock. The gray curve depicts the anisotropic positron-emission pattern at the moment of muon implantation. The pattern rotates rigidly with the muon spin (initially pointing towards the B detector) at an angular frequency  $\omega_\mu = \gamma_\mu B_{\text{ext}}$ . (B) Detected positron counts in the F and B detectors as a function of time after ca.  $10^7$  events. Inset: The asymmetry signal, obtained as the normalized difference between the F and B counts, eliminates the inessential exponential decay and highlights the signal decay (here assumed to be Gaussian) reflecting the nature of the sample.

precesses around  $B$  (see **Figure 1A**). (ii) In a longitudinal field (LF) configuration the applied field is parallel to  $S(0)$ , generally implying only a relaxing  $\mu$ SR signal.

Although, in principle, the TF scheme shown in **Figure 1A** works fine, strong transverse fields perpendicular to the muon momentum ( $p_\mu$ ) would deviate the muon beam too much from its original path. The Lorentz force can be zeroed by applying the field along the muon momentum. At the same time, to maintain the transverse geometry, the initial muon spin is rotated by  $90^\circ$  (in the  $x$  or  $y$  direction) by using a so-called Wien filter, consisting of crossed electric and magnetic fields. Such a configuration is also known as transverse muon-spin mode, while **Figure 1A** plots the longitudinal muon-spin mode (i.e.,  $p_\mu \parallel S_\mu$ ).

Since muons are uniformly implanted in the sample, they can detect the coexistence of different domains, characterized by distinct  $P_i(t)$  functions, whose amplitudes  $A_i$  represent a measure of the respective *volume fractions*. In case of superconductors, one can thus extract the SC volume fraction. More importantly, in a TF- $\mu$ SR experiment one can directly probe the SC flux-line lattice (FLL). In this case, at the onset of superconductivity, the muon-spin precession in a TF field loses coherence, reflecting the magnetic field modulation (i.e., broadening) due to the FLL. The shape of the field distribution arising from the FLL can be analyzed and eventually used to extract the magnetic penetration depth  $\lambda$  and the coherence length  $\xi$  [32]. In many type-II superconductors, the simple relation,  $\sigma_{\text{sc}}^2/\gamma_\mu^2 = 0.00371\Phi_0^2/\lambda_{\text{eff}}^4$ , connects the muon-spin depolarization rate in the superconducting phase,  $\sigma_{\text{sc}}$ , with the effective magnetic penetration depth,  $\lambda_{\text{eff}}$  (here  $\Phi_0$  is the magnetic flux quantum) [33, 34]. In case of superconductors with relatively low upper critical fields, the effects of the overlapping vortex cores with increasing field ought to be considered when extracting the magnetic penetration depth  $\lambda_{\text{eff}}$  from  $\sigma_{\text{sc}}$ . Since  $\lambda(T)$  is sensitive to the low-energy excitations, its evolution with temperature is intimately related to the structure of the superconducting gap. Hence,  $\mu$ SR allows us to directly study the *symmetry* and *value* of the superconducting gap.

More in detail, in a TF- $\mu$ SR experiment, the time evolution

of the asymmetry can be modeled by:

$$A_{\text{TF}}(t) = \sum_{i=1}^n A_i \cos(\gamma_\mu B_i t + \phi) e^{-\sigma_i^2 t^2/2} + A_{\text{bg}} \cos(\gamma_\mu B_{\text{bg}} t + \phi). \quad (2)$$

Here  $A_i$ ,  $A_{\text{bg}}$  and  $B_i$ ,  $B_{\text{bg}}$  are the asymmetries and local fields sensed by implanted muons in the sample and the sample holder,  $\gamma_\mu$  is the muon gyromagnetic ratio,  $\phi$  is a shared initial phase, and  $\sigma_i$  is the Gaussian relaxation rate of the  $i$ th component. The number of required components is material dependent, typically in the  $1 \leq n \leq 5$  range. In general, for superconductors with a large Ginzburg-Landau parameter  $\kappa$  ( $\gg 1$ ), the magnetic penetration depth is much larger than the coherence length. Hence, the field profiles of each fluxon overlap strongly, implying a narrow field distribution. Consequently, a single-oscillating component is sufficient to describe  $A(t)$ . In case of a small  $\kappa$  ( $\geq 1/\sqrt{2}$ ), the magnetic penetration depth is comparable with the coherence length. The rather small penetration depth implies fast-decaying fluxon field profiles and a broad field distribution, in turn requiring multiple oscillations to describe  $A(t)$ . The choice of  $n$  can be determined from the fast-Fourier-transform (FFT) spectra of the TF- $\mu$ SR, which is normally used to evaluate the goodness of the fits. In case of multi-component oscillations, the first term in Equation (2) describes the field distribution as the sum of  $n$  Gaussian relaxations [35]:

$$p(B) = \gamma_\mu \sum_{i=1}^n \frac{A_i}{\sigma_i} \exp\left[-\frac{\gamma_\mu^2 (B - B_i)^2}{2\sigma_i^2}\right]. \quad (3)$$

The first- and second moments of the field distribution in the sample can be calculated by:

$$\langle B \rangle = \sum_{i=1}^n \frac{A_i B_i}{A_{\text{tot}}} \quad \text{and} \quad \langle B^2 \rangle = \frac{\sigma_{\text{eff}}^2}{\gamma_\mu^2} = \sum_{i=1}^n \frac{A_i}{A_{\text{tot}}} \left[ \frac{\sigma_i^2}{\gamma_\mu^2} + (B_i - \langle B \rangle)^2 \right], \quad (4)$$

where  $A_{\text{tot}} = \sum_{i=1}^n A_i$ . The total Gaussian relaxation rate  $\sigma_{\text{eff}}$  in Equation (4) includes contributions from both a temperature-independent relaxation, due to nuclear moments ( $\sigma_n$ ), and a temperature-dependent relaxation, related to the FLL in the superconducting state ( $\sigma_{\text{sc}}$ ). The

$\sigma_{\text{sc}}$  values are then extracted by subtracting the nuclear contribution following  $\sigma_{\text{sc}} = \sqrt{\sigma_{\text{eff}}^2 - \sigma_{\text{n}}^2}$ .

To get further insights into the superconducting gap value and its symmetry, the temperature-dependent superfluid density  $\rho_{\text{sc}}(T)$  [proportional to  $\lambda_{\text{eff}}^{-2}(T)$ ] is often analyzed by using a general model:

$$\rho_{\text{sc}}(T) = \frac{\lambda_0^2}{\lambda_{\text{eff}}^2(T)} = 1 + 2 \left\langle \int_{\Delta_k}^{\infty} \frac{E}{\sqrt{E^2 - \Delta_k^2}} \frac{\partial f}{\partial E} dE \right\rangle_{\text{FS}}. \quad (5)$$

Here,  $\lambda_0$  is the effective magnetic penetration depth in the 0-K limit,  $f = (1 + e^{E/k_{\text{B}}T})^{-1}$  is the Fermi function and  $\langle \rangle_{\text{FS}}$  represents an average over the Fermi surface [36].  $\Delta_k(T) = \Delta(T)A_k$  is an angle-dependent gap function, where  $\Delta$  is the maximum gap value and  $A_k$  is the angular dependence of the gap, equal to 1,  $\cos 2\phi$ , and  $\sin \theta$  for an  $s$ -,  $d$ -, and  $p$ -wave model, respectively, with  $\phi$  and  $\theta$  being the azimuthal angles. The temperature dependence of the gap is assumed to follow the relation  $\Delta(T) = \Delta_0 \tanh\{1.82[1.018(T_{\text{c}}/T - 1)]^{0.51}\}$  [36, 37], where  $\Delta_0$  is the 0-K gap value.

### C. Zero-field $\mu\text{SR}$

A particular case of LF is that of zero-field (ZF)  $\mu\text{SR}$ , characterized by the absence of an external magnetic field. In this configuration the frequency of the  $\mu\text{SR}$  signal is exclusively proportional to the internal magnetic field, making it possible to determine the size of the ordered moments and, hence, the magnetic order parameter. Unlike various techniques, which require an external field to polarize the probe,  $\mu\text{SR}$  is unique in its capability of studying materials unperturbed by externally applied fields and in accessing their spontaneous magnetic fields. Due to the large muon magnetic moment ( $\mu_{\mu} = 8.89 \mu_{\text{N}}$ ), ZF- $\mu\text{SR}$  can sense even very small internal fields ( $\sim 10^{-2}$  mT), hence probing local magnetic fields of either nuclear or electronic nature. In addition, since the muon is an elementary spin-1/2 particle, it acts as a purely magnetic probe, i.e., free of quadrupole interactions. All these features, make ZF- $\mu\text{SR}$  an ideal technique for detecting TRS breaking in the superconducting state. This corresponds to the appearance (at the onset of SC) of spontaneous magnetic moments, whose magnitude can be very small, often lacking a proper magnetic order. As we show further on, in case of TRS breaking, we expect the appearance of an additional enhancement of relaxation below  $T_{\text{c}}$ , reflecting the occurrence of these weak spontaneous fields. During the ZF- $\mu\text{SR}$  measurements, to exclude the possibility of stray magnetic fields (typically larger than the weak internal fields), the magnets are quenched before starting the measurements, and an active field-nulling facility is used to compensate for stray fields down to  $1 \mu\text{T}$ .

If the amplitudes of the local fields reflect a Gaussian distribution with zero average (a rather common circumstance), the  $\mu\text{SR}$  signal consists of overlapping oscillations with different frequencies. While at short times the spin dephasing is limited, at long times it becomes relevant and gives rise to a so-called Kubo-Toyabe (KT) relaxation function [31, 38]. Two different models are frequently used to

analyze the ZF- $\mu\text{SR}$  data:

$$A_{\text{ZF}} = A_{\text{s}} \left[ \frac{1}{3} + \frac{2}{3} (1 - \sigma_{\text{ZF}}^2 t^2 - \Lambda_{\text{ZF}} t) e^{\left(-\frac{\sigma_{\text{ZF}}^2 t^2}{2} - \Lambda_{\text{ZF}} t\right)} \right] + A_{\text{bg}}, \quad (6)$$

or

$$A_{\text{ZF}} = A_{\text{s}} \left[ \frac{1}{3} + \frac{2}{3} (1 - \sigma_{\text{ZF}}^2 t^2) e^{-\frac{\sigma_{\text{ZF}}^2 t^2}{2}} \right] e^{-\Lambda_{\text{ZF}} t} + A_{\text{bg}}. \quad (7)$$

Equation (6) is also known as a combined Gaussian- and Lorentzian Kubo-Toyabe function, with the additional exponential relaxation describing the electronic contributions present in many real materials. In polycrystalline samples, the 1/3-non-relaxing and the 2/3-relaxing components of the asymmetry correspond to the powder average of the internal fields with respect to the initial muon-spin direction (statistically, with a 1/3 probability, the directions of the muon spin and of the local field coincide). Clearly, in case of single crystals, such prefactors might be different. The  $\sigma_{\text{ZF}}$  and  $\Lambda_{\text{ZF}}$  represent the zero-field Gaussian and Lorentzian relaxation rates, respectively. Typically,  $\Lambda_{\text{ZF}}$  shows an almost temperature-independent behavior. Hence, an increase of  $\sigma_{\text{ZF}}$  across  $T_{\text{c}}$  can be attributed to the spontaneous magnetic fields which break the TRS, as e.g., in ReT [17, 18, 20]. In case of diluted nuclear moments,  $\sigma_{\text{ZF}}$  is practically zero, hence, the TRS breaking is reflected in an increase of  $\Lambda_{\text{ZF}}$  below  $T_{\text{c}}$ , as e.g., in Zr<sub>3</sub>Ir and CaPtAs [16, 22].

### III. Re-BASED SUPERCONDUCTORS

In this section, we review the different phases of the binary ReT alloys. These are obtained when rhenium reacts with various early transition metals (see **Figure 2A**) and show rich crystal structures. Representative examples are shown in **Figures 2C–F**, including the hexagonal hcp-Mg- ( $P6_3/mmc$ , No. 194), cubic  $\alpha$ -Mn- ( $I\bar{4}3m$ , No. 217), tetragonal  $\beta$ -CrFe- ( $P4_2/mnm$ , No. 136), and cubic bcc-W-type ( $Im\bar{3}m$ , No. 229). Among these the cubic  $\alpha$ -Mn-type structure is noncentrosymmetric, while the rest are centrosymmetric [39]. Besides the above cases, a few other crystal structures have also been reported, including the cubic CsCl- ( $Pm\bar{3}m$ , No. 221), cubic Cr<sub>3</sub>Si- ( $Pm\bar{3}n$ , No. 223), and trigonal Mn<sub>21</sub>Zn<sub>25</sub>-type ( $R\bar{3}c$ , No. 167) [39]. As for the pure elements listed in **Figure 2A**, both Re and Os have an hcp-Mg-type structure, and show superconductivity below 2.7 and 0.7 K, respectively [20, 40]; while  $\nabla$ , Nb, Mo, Ta, and W all adopt a bcc-W-type structure, and become superconductors at  $\sim 5.4, 9.0, 1.0, 4.5,$  and  $0.015$  K, respectively [40]. Unlike the above cases, Ti, Zr, and Hf can form either high-temperature bcc-W-type or low-temperature hcp-Mg-type structures, with  $T_{\text{c}} \sim 0.4, 0.6,$  and  $0.13$  K, respectively [40].

For  $T = \text{Ti}$  3d metal, the known binary compounds are Re<sub>24</sub>Ti<sub>5</sub>, Re<sub>6</sub>Ti, and ReTi [42, 43]. The former two adopt a noncentrosymmetric  $\alpha$ -Mn-type structure and become superconductors below  $T_{\text{c}} = 6$  K [19, 40, 44], while the latter one crystallizes in a cubic CsCl-type structure. To date, no detailed physical properties have been reported for ReTi. For  $T = \nabla$ , superconductivity has been reported in hcp-Mg-type Re<sub>0.9</sub>V<sub>0.1</sub> ( $T_{\text{c}} = 9.4$  K),  $\beta$ -CrFe-type Re<sub>0.76</sub>V<sub>0.24</sub> ( $T_{\text{c}} = 4.5$  K), and bcc-W-type Re<sub>0.6</sub>V<sub>0.4</sub> ( $T_{\text{c}} = 2.2$  K) [40, 45]. Also for them, to date a microscopic study of their SC is still missing. The cubic Cr<sub>3</sub>Si-type Re<sub>0.71</sub>V<sub>0.29</sub> has also been synthesized, but its physical properties were never characterized [46].

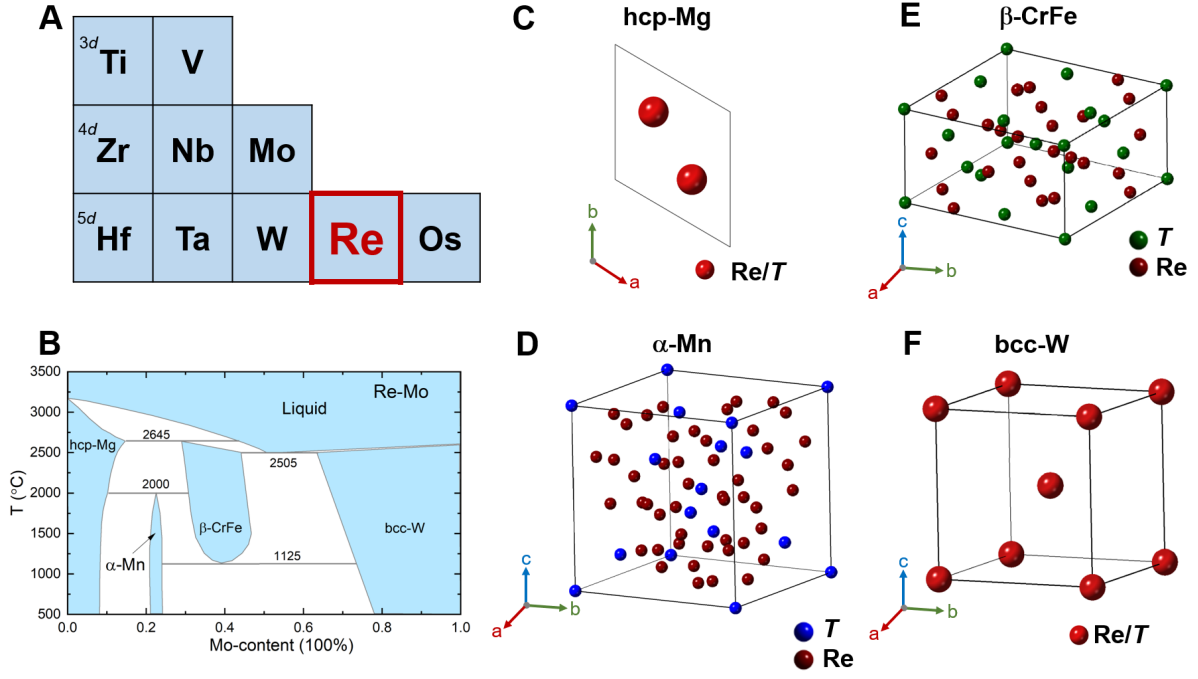


FIG. 2. Crystal structures of rhenium transition-metal (ReT) superconductors. (A) List of 3d, 4d, and 5d early transition metals, which can react with rhenium to form different crystal structures. (B) Binary phase diagram for the typical case of Re-Mo alloys (data adopted from Ref. [39]). (C–F) Unit cells of four most representative crystal structures of ReT binary compounds. Among these the cubic  $\alpha$ -Mn type ( $I\bar{4}3m$ , No. 217) in (D) is noncentrosymmetric, while the hexagonal hcp-Mg ( $P6_3/mmc$ , No. 194), tetragonal  $\beta$ -CrFe ( $P4_2/mnm$ , No. 136), and cubic bcc-W ( $Im\bar{3}m$ , No. 229) are centrosymmetric. The atomic coordinates for each structure can be found in Refs. [26, 41].

For  $T = \text{Zr}$  4d metal, the  $\alpha$ -Mn-type  $\text{Re}_{24}\text{Zr}_5$  ( $T_c = 5$  K) and  $\text{Re}_6\text{Zr}$  ( $T_c = 6.7$  K) have been investigated via both nuclear quadrupole resonance and  $\mu\text{SR}$  techniques [17, 47]. Except for the  $\alpha$ -Mn-type Re-Zr alloys, the  $\text{MgZn}_2$ -type  $\text{Re}_2\text{Zr}$  (similar to hcp-Mg-type) and  $\text{Mn}_{21}\text{Zn}_{25}$ -type  $\text{Re}_{25}\text{Zr}_{21}$  have been synthesized [39].  $\text{Re}_2\text{Zr}$  exhibits a  $T_c$  value of  $\sim 6$ –7 K [40, 48], while  $\text{Re}_{25}\text{Zr}_{21}$  has not been studied. For  $T = \text{Nb}$ , depending on Re/Nb concentration, four different solid phases including hcp-Mg-,  $\alpha$ -Mn-,  $\beta$ -CrFe-, and bcc-W-type have been reported. On the Re-rich side, the hcp-Mg-type Re-Nb alloys are limited to less than 3% Nb concentration [39], whereas many  $\alpha$ -Mn-type Re-Nb binary alloys have been grown and widely studied by various techniques [20, 49–52], with the highest  $T_c$  reaching 8.8 K in  $\text{Re}_{24}\text{Nb}_5$  (denoted as  $\text{Re}_{0.82}\text{Nb}_{0.18}$  in the original paper [20]). At intermediate Re/Nb values, for example, in  $\beta$ -CrFe-type  $\text{Re}_{0.55}\text{Nb}_{0.45}$ ,  $T_c$ s in the range of 2 to 4 K [40] have been reported, but no microscopic studies yet. As for the Nb-rich side (Nb concentration larger than 60%), here the Re-Nb alloys exhibit the same structure as that of pure Nb, but much lower  $T_c$  values than Nb [39, 40]. For  $T = \text{Mo}$ , the binary Re-Mo phase diagram (see Figure 2B) covers also four different solid phases [39]. The binary Re-Mo alloys have been characterized by different techniques and all of them shown to become superconductors at low temperature [26, 27]. The  $T_c$  varies nonmonotonically upon changing the Mo concentration, giving rise to three distinct superconducting regions. On the Re-rich side, the first SC region shows the highest  $T_c \sim 9.4$  K in the hcp-Mg-type  $\text{Re}_{0.77}\text{Mo}_{0.23}$ . The same material but with an  $\alpha$ -Mn-type structure can also be grown, with a  $T_c$  value about 1 K lower than the hcp-Mg-type. In the second superconducting region, where the alloys adopt a  $\beta$ -CrFe-type structure, the superconducting transition tem-

perature  $T_c \sim 6.3$  K is almost independent of Mo content. Finally, on the Mo-rich side, all Re-Mo alloys display a cubic bcc-W-type structure and form a third superconducting region with the highest  $T_c$  reaching 12.4 K in  $\text{Re}_{0.4}\text{Mo}_{0.6}$ .

For  $T = \text{Hf}$  5d metal, the Re-Hf alloys show a similar phase diagram to Re-Zr. With only  $\sim 3\%$  Hf substitution,  $T_c$  increases from  $< 3$  K to 7.3 K in the hcp-Mg-type Re-Hf alloys [40]. Both the  $\alpha$ -Mn-type  $\text{Re}_6\text{Hf}$  and the  $\text{MgZn}_2$ -type  $\text{Re}_2\text{Hf}$  become superconductors below  $T_c \sim 6$  K [18, 40, 48, 53, 54], whereas the physical properties of  $\text{Mn}_{21}\text{Zn}_{25}$ -type  $\text{Re}_{25}\text{Hf}_{21}$  remain largely unknown. On the Hf-rich side, the bcc-W-type alloys exhibit relatively low  $T_c$ s, e.g.,  $T_c = 1.7$  K for  $\text{Hf}_{0.875}\text{Re}_{0.125}$  [40]. For  $T = \text{Ta}$ , although the four different structures shown in Figure 2C–F can be synthesized, only the  $\alpha$ -Mn-type Re-Ta alloys have been well studied. For example,  $\text{Re}_3\text{Ta}$  and  $\text{Re}_{5.5}\text{Ta}$  show  $T_c$  values of 4.7 K and 8 K, respectively [55, 56]. On the Ta-rich side, the bcc-W-type Re-Ta alloys become superconducting at  $T_c < 3.5$  K, lower than the  $T_c$  of pure Ta [57]. We note that in case of the  $\beta$ -CrFe-type Re-Ta alloys, no superconducting transition has been observed down to 1.8 K in either  $\text{Re}_{0.5}\text{Ta}_{0.5}$  or  $\text{Re}_{0.6}\text{Ta}_{0.4}$ . For  $T = \text{W}$ , the Re-W alloys show a very similar phase diagram to Re-Mo in Figure 2B. As the W concentration increases, the highest  $T_c$  values reach  $\sim 8, 9, 6,$  and  $5$  K in the hcp-Mg-,  $\alpha$ -Mn-,  $\beta$ -CrFe-, and the bcc-W-type alloys, respectively [39, 40]. Among them, only the hcp-Mg- and the  $\alpha$ -Mn-type  $\text{Re}_3\text{W}$  have been investigated [25, 58]. Finally, in case of  $T = \text{Os}$ , the Re-Os alloys show a rather monotonous phase diagram, since only hcp-Mg-type compounds with  $T_c$  values below 2 K can be synthesized [39, 40].

#### IV. UPPER CRITICAL FIELD AND NODELESS SUPERCONDUCTIVITY

As mentioned in the introduction, due to the mixture of singlet- and triplet pairing, some NCSCs may exhibit relatively high upper critical fields, often very close to or even exceeding the Pauli limit, as e.g., CePt<sub>3</sub>Si [12], Ce(Rh,Ir)Si<sub>3</sub> [59, 60], and recently (Ta,Nb)Rh<sub>2</sub>B<sub>2</sub> [61]. Therefore, the upper critical field can provide valuable clues about the nature of superconductivity. To investigate the temperature evolution of the upper critical field  $H_{c2}(T)$ , in general, the temperature- (or field-) dependent electrical resistivity  $\rho$ , magnetic susceptibility  $\chi$ , and specific heat  $C/T$  at various magnetic fields (or at various temperatures) are measured [19, 20, 27]. As an example, **Figure 3A** shows the  $H_{c2}(T)$  for Re<sub>24</sub>Nb<sub>5</sub> ( $\alpha$ -Mn-type) and Re<sub>0.4</sub>Mo<sub>0.6</sub> (bcc-W-type) versus the normalized temperature  $T/T_c(0)$ . To obtain the upper critical field in the zero-temperature limit,  $H_{c2}(0)$ , the Werthamer-Helfand-Hohenberg (WHH) or the Ginzburg-Landau (GL) models are usually applied when analyzing the  $H_{c2}(T)$  data of Re $T$  superconductors. Both models can adequately describe single-gap superconductors. Here, in case of Re<sub>24</sub>Nb<sub>5</sub> and Re<sub>0.4</sub>Mo<sub>0.6</sub>, the WHH model (solid line in **Figure 3A**) reproduces the data very well and gives  $\mu_0 H_{c2}(0) = 15.6$  T, and 3.08 T, respectively. **Figure 3B** summarizes the  $\mu_0 H_{c2}(0)$  values of the Re $T$  and  $\alpha$ -Mn-type NbOs<sub>2</sub> superconductors. As discussed in Section III, most of the previous studies focused exclusively on  $\alpha$ -Mn-type Re $T$  superconductors being practically neglected and requiring further studies. Unlike other Re $T$ , all Re-Mo alloys belonging to four different structures have been studied via macro- and microscopic techniques [26, 27]. The  $\mu_0 H_{c2}(0)$  of centrosymmetric Re-Mo alloys, including hcp-Mg-,  $\beta$ -CrFe-, and bcc-W-type, are far away from the Pauli limit  $\mu_0 H_P = 1.86 T_c$  (indicated by a dashed line in **Figure 3B**). Conversely, the  $\alpha$ -Mn-type Re $T$  and NbOs<sub>2</sub> both exhibit large upper critical fields, very close to or even exceeding the Pauli limit, despite their different  $T_c$  values. For example,  $\mu_0 H_{c2}(0) = 15.6$  and 16.5 T for Re<sub>24</sub>Nb<sub>5</sub> and Re<sub>5.5</sub>Ta, while their  $\mu_0 H_P(0)$  are 16.4 and 14.9 T, respectively. The hcp-Mg-type Re<sub>3</sub>W also exhibits a relatively high  $H_{c2}$ , as determined from electrical resistivity data. However, its  $H_{c2}$  value might be overestimated since, e.g., at 9 T, no zero resistivity could be observed down to 2 K. Therefore, other bulk techniques, including magnetization- or heat capacity measurements are required to determine the intrinsic  $H_{c2}$ . In general, it would be interesting to know the  $H_{c2}$  values of other centrosymmetric Re $T$  superconductors. Overall, the upper critical fields in **Figure 3B** indicate the possibility of singlet-triplet mixing in the noncentrosymmetric  $\alpha$ -Mn-type superconductors.

Transverse-field  $\mu$ SR represents one of the most powerful techniques to investigate the superconductivity at a microscopic level. To illustrate this, in the inset of **Figure 3C** we show two typical TF- $\mu$ SR spectra for bcc-W-type Re<sub>0.4</sub>Mo<sub>0.6</sub> in the normal and the superconducting states. Below  $T_c$ , the fast decay induced by FLL (encoded into  $\sigma_{sc}$ ) is clearly visible, while the slow decay in the normal state is attributed to the randomly oriented nuclear magnetic moments. By comparing the two spectra, one can also determine the superconducting volume fraction of a superconductor. As an example, the main panel of **Figure 3C** shows the normalized superfluid density calculated from  $\sigma_{sc}(T)$ , which is proportional to  $[\lambda(T)/\lambda(0)]^{-2}$  (see details in Section II B), as a

function of the reduced temperature  $T/T_c(0)$  for Re<sub>24</sub>Nb<sub>5</sub> and Re<sub>0.4</sub>Mo<sub>0.6</sub> [20, 27]. The low- $T$  superfluid density is practically independent of temperature, clearly suggesting a lack of low-energy excitations and a fully-gapped superconductivity. Contrarily, such excitations exist in case of nodes in the superconducting gap, implying a temperature-dependent superfluid density below  $\sim T_c/3$ . As shown by solid lines in **Figure 3C**, the  $\rho_{sc}(T)$  of Re $T$  superconductors is described very well by a fully-gapped  $s$ -wave model (see Equation 5). The other  $\alpha$ -Mn-type Re $T$ , TaOs, and NbOs<sub>2</sub> exhibit similar temperature-invariant superfluid densities [17–19, 25, 44, 56, 62, 63]. Although Re $T$  alloys adopt different crystal structures (i.e., centrosymmetric or noncentrosymmetric, see **Figure 2C–F**) and have different  $T_c$  values, they regularly exhibit low- $T$  superfluid densities which are independent of temperature [27]. Except for  $T = \text{Mo}$  (and for some  $\alpha$ -Mn structures), a systematic microscopic study of superconductivity in other Re $T$  superconductors is still missing. Clearly, it would be interesting to know if their SC behavior is similar to that of Re-Mo alloys. The nodeless SC scenario in Re $T$  alloys is also supported by other techniques, as the electronic specific heat, the magnetic penetration depth measured via the tunnel-diode-oscillator-based technique, or the point-contact Andreev reflection [19, 20, 27, 53, 54, 58, 64–66]. In addition, some studies have found evidence of two-gap superconductivity in Re<sub>0.82</sub>Nb<sub>0.18</sub> and Re<sub>6</sub>Zr [49, 66].

**Figure 3D** summarizes the zero-temperature superconducting energy gap value for Re $T$  and  $\alpha$ -Mn-type NbOs<sub>2</sub> and TaOs superconductors as a function of their critical temperatures. Most of them exhibit a  $\Delta_0/k_B T_c$  ratio larger than 1.76 (see dashed line in **Figure 3D**), the value expected for a weakly coupled BCS superconductor, which indicates a moderately strong coupling in these superconductors. In addition, the specific-heat discontinuity at  $T_c$  (i.e.,  $\Delta C/\gamma T_c$ ) is larger than the conventional BCS value of 1.43, again indicating an enhanced electron-phonon coupling [19, 20, 27, 53, 54, 58, 64]. As mentioned above, it is worth noting that the superconducting parameters of all the other Re $T$  materials (except for  $\alpha$ -Mn-type and  $T = \text{Mo}$ ) are missing, prompting further research efforts in this direction.

As discussed in the introduction, the lack of inversion symmetry in the NCSCs often induces an ASOC. This splits the Fermi surface by lifting the degeneracy of the conduction electrons, thus allowing admixtures of spin-singlet and spin-triplet pairing. In general, the strength of ASOC determines the degree of such an admixture and thus the superconducting properties of NCSCs [1, 2]. A fully-gapped superconductor (i.e., dominated by spin-singlet pairing) can be tuned into a nodal superconductor (dominated by spin-triplet pairing) by increasing the strength of ASOC. Such mechanism has been successfully demonstrated, e.g., in weakly-correlated Li<sub>2</sub>Pt<sub>3</sub>B ( $E_{\text{SOC}}/k_B T_c \sim 831$ ) [67, 68], CaPtAs ( $E_{\text{SOC}}/k_B T_c \sim 800$ ) [16, 69], and in strongly-correlated CePt<sub>3</sub>Si ( $E_{\text{SOC}}/k_B T_c \sim 3095$ ) superconductors [12, 70], all exhibiting a relatively large band splitting  $E_{\text{SOC}}$  compared to their superconducting energy scale  $k_B T_c$ . In the  $\alpha$ -Mn-type Re $T$  alloys, the density of states (DOS) near the Fermi level is dominated by the 5d orbitals of rhenium atoms, while contributions from the  $d$  orbitals of  $T$  atoms are negligible [71–73]. Therefore, a possible enhancement of SOC due to 3d-(e.g., Ti, V) up to 5d-electrons (e.g., Hf, Ta, W, Os) will, in principle, neither increase the band splitting  $E_{\text{SOC}}$  nor affect the pairing admixture and thus the superconducting properties of  $\alpha$ -Mn-type Re $T$  superconductors. According to

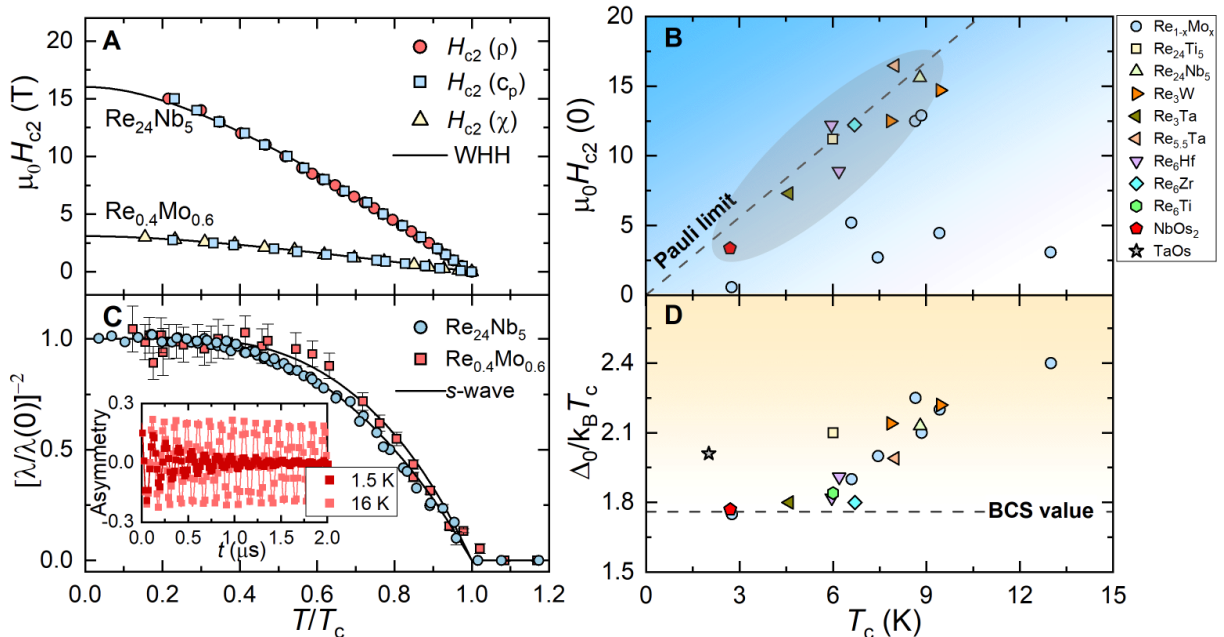


FIG. 3. Upper critical field and superconducting energy gap. **(A)** The upper critical field  $H_{c2}$ , as determined from electrical resistivity-, heat capacity-, and magnetic susceptibility measurements, as a function of the reduced superconducting transition temperature  $T_c/T_c(0)$  for  $\text{Re}_{24}\text{Nb}_5$  and  $\text{Re}_{0.4}\text{Mo}_{0.6}$ . Solid-lines represent fits to the Werthamer-Helfand-Hohenberg (WHH) model. **(B)** Zero-temperature  $H_{c2}$  versus the superconducting transition temperature  $T_c$  for  $\alpha$ -Mn-type  $\text{NbOs}_2$  and all  $\text{Re}T$  superconductors. The shaded region in **(B)** marks the noncentrosymmetric  $\alpha$ -Mn type superconductors, while the dashed line indicates the Pauli limit (i.e.,  $\mu_0 H_p = 1.86 T_c$ ). **(C)** Superfluid density vs reduced temperature  $T_c/T_c(0)$  for  $\text{Re}_{24}\text{Nb}_5$  and  $\text{Re}_{0.4}\text{Mo}_{0.6}$ . Lines are fits to a fully-gapped  $s$ -wave model. The insert shows the TF- $\mu$ SR spectra for  $\text{Re}_{0.4}\text{Mo}_{0.6}$  measured in a field of 60 mT in the normal- (16 K) and the superconducting state (1.5 K). Solid lines are fits to Equation 2. **(D)** Zero-temperature superconducting energy gap  $\Delta_0$  (in  $k_B T_c$  units) as a function of  $T_c$  for  $\text{Re}T$  and  $\alpha$ -Mn-type  $\text{NbOs}_2$  and  $\text{TaOs}$  superconductors. Here, the dashed line represents the BCS superconducting gap in the weak-coupling limit (i.e.,  $1.76 k_B T_c$ ). Data were taken from Refs. [17–20, 25, 27, 44, 53, 54, 56, 58, 62–64].

band-structure calculations, in  $\text{Re}_6\text{Zr}$ , the SOC-induced band splitting is about 30 meV [73], implying a very small ratio  $E_{\text{SOC}}/k_B T_c \sim 25$ , comparable to that of fully-gapped  $\text{Li}_2\text{Pd}_3\text{B}$ ,  $\text{Mo}_3\text{P}$ , and  $\text{Zr}_3\text{Ir}$  superconductors [22, 68, 74]. Therefore, despite the relatively large SOC of rhenium atoms, its effects are too weak to significantly influence the bands near the Fermi level. This might explain why all the  $\alpha$ -Mn-type  $\text{Re}T$  superconductors exhibit nodeless superconductivity, more consistent with a spin-singlet dominated pairing [17–20, 25, 55]. However, we recall that often, due to the similar magnitude and same-sign of the order parameter on the spin-split Fermi surfaces, a possible mixed-pairing superconductor may be challenging to detect or to distinguish from a single-gap  $s$ -wave superconductor [75]. The almost spherical symmetry of the Fermi surface in these materials may also explain their BCS-like superconducting states [72]. As for the other centrosymmetric  $\text{Re}T$  alloys, in most of them the Re and  $T$  atoms occupy the same atomic positions in the unit cell. In this case, as the  $T$ -content increases, the contribution of  $T$   $d$  orbitals to the DOS is progressively enhanced, at the expense of the Re  $5d$  orbitals. Therefore, the chemical substitution of Re by another  $3d$ ,  $4d$ , or  $5d$   $T$  metal (see Figure 2), should significantly tune the SOC and, hence, the band splitting, an interesting hypothesis waiting for theoretical confirmation. However, even for  $T = \text{Hf}$ ,  $\text{Ta}$ ,  $\text{W}$ , and  $\text{Os}$ , the maximum  $E_{\text{SOC}}$  should still be comparable to that of  $\alpha$ -Mn-type  $\text{Re}T$  alloys. Finally, irrespective of the strength of SOC, due to their centrosymmetric crystal structures, these compounds may exhibit either singlet- or triplet-pairing, but not an admixture of both. According to the TF- $\mu$ SR results (see Figure 3C), despite a change in SOC

and of the different crystal structures (see Figure 2C–F), all  $\text{Re}T$  superconductors exhibit fully-gapped superconducting states. This finding strongly suggests that, in the  $\text{Re}T$  superconductors, spin-singlet pairing is dominant.

## V. TIME-REVERSAL SYMMETRY BREAKING

Owing to its very high sensitivity (see details in Section II C), ZF- $\mu$ SR has been successfully used to search for spontaneous magnetic fields, reflecting the breaking of TRS in the superconducting states of different types of superconductors, as e.g.,  $\text{Sr}_2\text{RuO}_4$ ,  $\text{UPT}_3$ ,  $\text{PrOs}_4\text{Sb}_{12}$ ,  $\text{LaNiGa}_2$ ,  $\text{LaNiC}_2$ ,  $\text{La}_7(\text{Rh},\text{Ir})_3$ , and  $\alpha$ -Mn- $\text{Re}T$  [14, 15, 17–21, 76–81]. The latter three are typical examples of weakly-correlated NSCSs, to be contrasted with strongly-correlated NSCSs, where either the TRS is broken by a coexisting long-range magnetic order, or the tiny TRS-breaking signal is very difficult to detect due to the presence of strong magnetic fluctuations [28]. In the former case, the broken TRS is unrelated to the superconductivity, while in the later case, a genuine TRS breaking effect is masked by the much faster muon-spin relaxation caused by magnetic fluctuations. Therefore, in general, a TRS breaking effect is more easily (and reliably) detected in weakly-correlated- or non-magnetic superconductors using  $\mu$ SR techniques. Normally, in the absence of external fields, the onset of superconductivity does not imply changes in the ZF- $\mu$ SR relaxation rate. However, in presence of a broken TRS, the onset of a tiny spontaneous polarization or of currents gives rise to associated (weak) magnetic fields, readily detected by ZF- $\mu$ SR as an increase

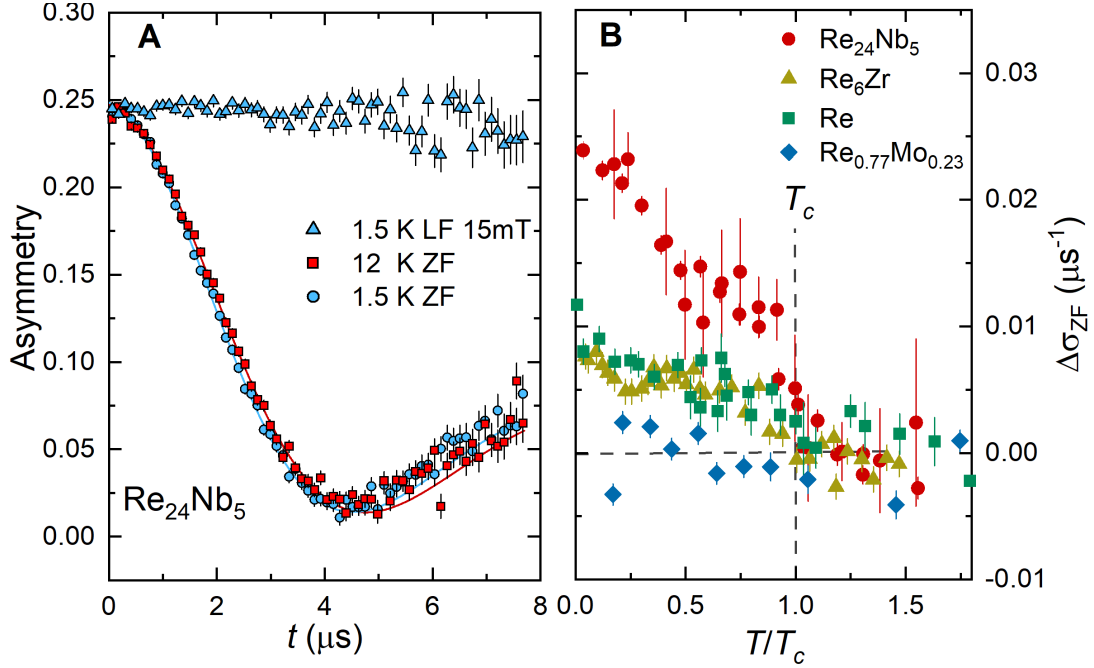


FIG. 4. ZF- $\mu$ SR and evidence for TRS breaking. (A) ZF- $\mu$ SR spectra for  $\text{Re}_{24}\text{Nb}_5$  collected in the superconducting and normal states. Top: additional  $\mu$ SR data collected at 1.5 K in a 15-mT longitudinal field, are also shown. The solid lines are fits using Equation 6. (B) Gaussian relaxation rate  $\Delta\sigma_{\text{ZF}}$  vs  $T/T_c$  for  $\text{Re}_{24}\text{Nb}_5$ ,  $\text{Re}_6\text{Zr}$ ,  $\text{Re}$ , and  $\text{Re}_{0.77}\text{Mo}_{0.23}$  — here  $\Delta\sigma_{\text{ZF}}(T) = \sigma_{\text{ZF}}(T) - \sigma_{\text{ZF}}(T > T_c)$ . While for the first three there is a clear increase of  $\Delta\sigma_{\text{ZF}}$  across  $T_c$  (hence a breaking of TRS), no changes occur in the last case (TRS is preserved). Data were taken from Refs. [17, 19, 20, 27].

in the relaxation rate. Given the tiny size of such effects, the ZF- $\mu$ SR measurements are usually performed in both the normal- and the superconducting state with a relatively high statistics, at least twice that of the TF- $\mu$ SR spectra. As an example, **Figure 4A** plots the ZF- $\mu$ SR spectra of  $\alpha$ -Mn-type  $\text{Re}_{25}\text{Nb}_5$ , with the other  $\text{Re}T$  superconductors showing a similar behavior. The ZF- $\mu$ SR spectra collected below and above  $T_c$  (at 1.5 and 12 K) exhibit small yet measurable differences. The lack of any oscillations in the spectra, implies the non-magnetic nature of  $\text{Re}T$  superconductors. Further, longitudinal-field  $\mu$ SR measurements under a relatively small applied field (typically a few tens of mT) in the superconducting state are usually performed to check if the applied field can fully decouple the muon spins from the weak spontaneous magnetic fields, and thus exclude extrinsic effects. In non-magnetic materials in the absence of external magnetic fields, the muon-spin relaxation is mostly determined by the interaction between the muon spins and the randomly oriented nuclear magnetic moments. Therefore, the spontaneous magnetic fields due to the TRS breaking will be reflected in an additional increase of muon-spin relaxation. The ZF- $\mu$ SR asymmetry can be described by means of a Gaussian- or a Lorentzian Kubo-Toyabe relaxation, or a combination thereof (see Equations 6 and 7). **Figure 4B** summarizes the Gaussian relaxation rate  $\sigma_{\text{ZF}}$  versus the reduced temperature  $T/T_c$  for the  $\alpha$ -Mn-type  $\text{Re}_{24}\text{Nb}_5$ ,  $\text{Re}_6\text{Zr}$ , and  $\text{Re}_{0.77}\text{Mo}_{0.23}$ , and the hcp-Mg-type elementary  $\text{Re}$ . Above  $T_c$ , all the samples show a temperature-independent  $\sigma_{\text{ZF}}$ . Except for  $\text{Re}_{0.77}\text{Mo}_{0.23}$ , a small yet clear increase of  $\sigma_{\text{ZF}}(T)$  below  $T_c$  indicates the onset of spontaneous magnetic fields, which represent the signature of TRS breaking in the superconducting state [17, 20, 27]. The other  $\alpha$ -Mn-type superconductors, e.g.,  $\text{Re}_6\text{Ti}$ , and  $\text{Re}_6\text{Hf}$  [18, 44], show similar  $\sigma_{\text{ZF}}(T)$  to  $\text{Re}_{24}\text{Nb}_5$  and  $\text{Re}_6\text{Zr}$ , and thus the breaking of TRS in the superconducting state. At the same time, in

the isostructural  $\text{Re}_3\text{Ta}$ ,  $\text{Re}_{5.5}\text{Ta}$ , and  $\text{Re}_3\text{W}$  cases, there is no clear increase in  $\sigma_{\text{ZF}}(T)$  upon crossing  $T_c$ , implying a preserved TRS [25, 55, 56].

Recently, the breaking of TRS and the presence of nodes in the SC gap, attributed to an admixture of singlet- and triplet pairing, has been reported in the noncentrosymmetric  $\text{CaPtAs}$  superconductor [16]. In general, however, the breaking of TRS in the superconducting state and a lack of space-inversion symmetry in the crystal structure are independent events, not necessarily occurring together. For instance, the unconventional spin-triplet pairing is expected to break TRS below  $T_c$ , as has been shown, e.g., in  $\text{Sr}_2\text{RuO}_4$ ,  $\text{Upt}_3$ , and  $\text{UTe}_2$  triplet superconductors [76–78, 80, 82–86]. An  $s + id$  spin-singlet state was proposed to account for the TRS breaking in some iron-based high- $T_c$  superconductors [87], where a nodal gap is also expected. The frequent occurrence of TRS breaking in the fully-gapped (i.e., dominated by spin-singlet pairing)  $\text{Re}T$  superconductors (see Section IV) is, therefore, rather puzzling. A similarly surprising result was the report that elementary rhenium also exhibits signatures of TRS breaking in its superconducting state (see **Figure 4B**), with  $\Delta\sigma_{\text{ZF}}(T)$  being comparable to that of  $\text{Re}_6\text{Zr}$  [20, 27]. Since elementary rhenium adopts a centrosymmetric hcp-Mg crystal structure (see **Figure 2C**), this indicates that a lack of inversion symmetry and the accompanying ASOC effects are not crucial factors for the occurrence of TRS breaking in  $\text{Re}T$  superconductors. Further on, a comparison of ZF- $\mu$ SR measurements on  $\text{Re}$ - $\text{Mo}$  alloys with different  $\text{Re}/\text{Mo}$  contents, covering almost all the crystal structures reported in **Figure 2**, shows that only  $\text{Re}$  and  $\text{Re}_{0.88}\text{Mo}_{0.12}$  exhibit a broken TRS in the superconducting state, while those with a higher  $\text{Mo}$ -content ( $\sim 23\%$ – $60\%$ ), including both the centrosymmetric- and noncentrosymmetric  $\text{Re}_{0.77}\text{Mo}_{0.23}$ , preserve the TRS. Considering the preserved TRS in  $\text{Mg}_{10}\text{Ir}_{19}\text{B}_{16}$ , and  $\text{Nb}_{0.5}\text{Os}_{0.5}$  [23, 24], all of



which share the same  $\alpha$ -Mn-type structure, this implies that TRS breaking in ReT superconductors is clearly not related to the noncentrosymmetric crystal structure or to a possible mixed pairing but, most likely, is due to the presence of rhenium and to its amount. Such conclusion is further reinforced by the preserved TRS in many Re-based superconductors, whose Re-content is below a certain threshold. Such cases include, e.g., Re<sub>3</sub>W, Re<sub>3</sub>Ta, Re-Mo (with Mo-content higher than 12%) [25, 27, 55], the recently reported Re-B superconductors [88], and the diluted ReBe<sub>22</sub> superconductor [89]. Moreover, by comparing the ZF- $\mu$ SR relaxation across various ReT superconductors, a clear positive correlation between  $\Delta\sigma_{ZF}$  (i.e., spontaneous fields) and the size of the nuclear magnetic moments  $\mu_n$  was identified [20]. For instance, among the ReT superconductors, Re<sub>24</sub>Nb<sub>5</sub> shows the largest spontaneous fields below  $T_c$  (see Figure 4B), a fact compatible with the large nuclear magnetic moment of niobium, practically twice that of rhenium (6.17 vs. 3.2  $\mu_N$ ). However, the correlation between  $\mu_n$  and  $\Delta\sigma_{ZF}$  alone cannot explain TRS breaking, considering that elementary Nb itself, despite having the highest  $\mu_n$ , does not break TRS. Clearly, the origin of such correlation is not yet understood and it requires further experimental and theoretical studies.

If SOC can be ignored, an alternative mechanism, which can account for the TRS breaking in ReT superconductors in presence of a fully-opened superconducting gap, is the internally-antisymmetric nonunitary triplet (INT) pairing. The INT pairing was originally proposed to explain the TRS breaking and nodeless SC in centrosymmetric LaNiGa<sub>2</sub> [3, 81, 90] and noncentrosymmetric LaNiC<sub>2</sub> [14, 91], both exhibiting a relatively weak SOC. In case of INT pairing, the superconducting pairing function is antisymmetric with respect to the orbital degree of freedom, while remaining symmetric in the spin- and crystal-momentum channels [14, 81, 90, 91]. Since in ReT superconductors, too, the SOC interaction is relatively weak ( $\sim 30$  meV, see Section IV) [73] and since neither TRS breaking nor the nodeless SC are related to the symmetry of ReT crystal structures, the effect of SOC to the observed TRS breaking is insignificant. This could, therefore, explain why a lack of inversion symmetry (essential to SOC) is not a precondition for TRS breaking in ReT superconductors. Moreover, the occurrence of an INT state relies on the availability of a local-pairing mechanism driven by Hund's rules, e.g., by Ni 3d-electrons in LaNiC<sub>2</sub> and LaNiGa<sub>2</sub> [3, 14, 81, 90, 91]. Such local-pairing mechanism may also occur in ReT superconductors, since rhenium too can be magnetic [92, 93]. This consideration is also in good agreement with the observation that TRS breaking depends on Re content, but not on a noncentrosymmetric crystal structure.

## VI. CONCLUSION

In this short review we focused on recent experimental studies of ReT superconductors, where time-reversal symmetry breaking effects are often present and whose superconductivity can, therefore, be considered as unconventional. Due to its high sensitivity to the weak internal fields associated with TRS breaking,  $\mu$ SR represents one of the key techniques in the search for TRS-breaking effects in the superconducting state. Nonetheless, in certain cases, the amplitude of the spontaneous magnetic fields (the fingerprint of TRS breaking) may still be below the resolution of the  $\mu$ SR

technique ( $\sim 10^{-2}$  mT). Hence, the future use of other techniques, e.g., based on the optical Kerr effect [11], another very sensitive probe of spontaneous fields in unconventional superconductors, remains crucial. Due to their rich crystal structures, covering both centro- and noncentrosymmetric cases, and the pervasive presence of superconductivity at low temperatures, the nonmagnetic Re-based materials are the ideal choice for investigating the origin of TRS breaking. Here, we reviewed different cases of Re-containing superconductors, ranging from elementary rhenium, to ReT ( $T = 3d-5d$  early transition metals), to the dilute-Re case of ReBe<sub>22</sub>, all of which were investigated through both macroscopic and microscopic techniques. By a comparative study of ReT with different T metals mostly using  $\mu$ SR technique, we could demonstrate the secondary role played by SOC and why the spin-singlet pairing is dominant in ReT superconductors. This, however, brings up the question of reconciling the occurrence of TRS breaking with a fully-gapped SC state (spin-singlet pairing). A possible solution to this is offered by the so-called INT model, which requires an antisymmetric pairing function involving the orbital degree of freedom, making it insensitive to the presence (or lack) of inversion symmetry and SOC. Overall, the reported results suggest that the rhenium presence and its amount are two key factors for the appearance and the extent of TRS breaking in the Re-based superconductors. These key observations, albeit important, demand new experimental and theoretical investigations to further generalize them.

To date, as nearly all current studies have focused exclusively on  $\alpha$ -Mn-type ReT superconductors (except for the Re-Mo series considered here), the superconducting properties of most other ReT alloys remain basically unexplored. Hence, the synthesis and characterization of non- $\alpha$ -Mn-type ReT alloys, including the study of their electrical, magnetic, and thermodynamic properties, is of clear interest. Similarly, systematic  $\mu$ SR measurements, crucial for detecting the presence of TRS breaking in Re-based superconductors, are in high demand. For instance, although both Re-Zr and Re-Nb alloys exhibit rich crystal structures and superconducting phase diagrams, only their  $\alpha$ -Mn-type phase has been explored. In addition, most of the original measurements were performed only on polycrystalline samples. Hence, the synthesis of single crystals will be essential in the comprehensive search for possible superconducting nodes and, thus, for mixed singlet-triplet pairing. Finally, it would be of interest to extend the  $\mu$ SR studies on elementary rhenium from the bulk- to its thin-film form, where inversion symmetry is artificially broken. By checking if the TRS breaking is maintained or not, will help us to further clarify the rhenium conundrum.

## CONFLICT OF INTEREST STATEMENT

The authors declare that the research was conducted in the absence of any commercial or financial relationships that could be construed as a potential conflict of interest.

## AUTHOR CONTRIBUTIONS

The manuscript was prepared and written by both the authors.

This work was supported by start funding from East-China Normal University (ECNU), the Swiss National Science Foundation (Grant No. 200021-169455) and the Sino-Swiss Science and Technology Cooperation (Grant No. IZLCZ2-170075).

We thank M. Shi for the fruitful discussion. We thank M. Medarde for the assistance during the electrical resistivity and magnetization measurements, and D. J. Gawryluk and E. Pomjakushina for synthesizing the materials. We acknowledge the allocation of beam time at the Swiss muon source ( $S\mu S$ ) (DOLLY, GPS, and LTF spectrometers).

*Note* This is the version of article after peer review but without editing, as submitted to *Frontiers in Physics*. Frontiers is not responsible for any errors or omissions in this version of the manuscript. The paper is available online at [10.3389/fphy.2021.651163](https://doi.org/10.3389/fphy.2021.651163).

- 
- [1] E. Bauer and M. Sigrist, eds., *Non-Centrosymmetric Superconductors*, Vol. 847 (Springer Verlag, Berlin, 2012).
- [2] M. Smidman, M. B. Salamon, H. Q. Yuan, and D. F. Agterberg, Superconductivity and spin-orbit coupling in non-centrosymmetric materials: A review, *Rep. Prog. Phys.* **80**, 036501 (2017).
- [3] S. K. Ghosh, G. Csire, P. Whittlesea, J. F. Annett, M. Gradhand, B. Újfalussy, and J. Quintanilla, Quantitative theory of triplet pairing in the unconventional superconductor  $\text{LaNiGa}_2$ , *Phys. Rev. B* **101**, 100506 (2020).
- [4] H. Kim, K. Wang, Y. Nakajima, R. Hu, S. Ziemak, P. Syers, L. Wang, H. Hodovanets, J. D. Denlinger, P. M. R. Brydon, D. F. Agterberg, M. A. Tanatar, R. Prozorov, and J. Paglione, Beyond triplet: Unconventional superconductivity in a spin-3/2 topological semimetal, *Sci. Adv.* **4**, eaao4513 (2018).
- [5] Z. X. Sun, M. Enayat, A. Maldonado, C. Lithgow, E. Yelland, D. C. Peets, A. Yaresko, A. P. Schnyder, and P. Wahl, Dirac surface states and nature of superconductivity in noncentrosymmetric  $\text{BiPd}$ , *Nat. Commun.* **6**, 6633 (2015).
- [6] M. N. Ali, Q. D. Gibson, T. Klimczuk, and R. J. Cava, Noncentrosymmetric superconductor with a bulk three-dimensional Dirac cone gapped by strong spin-orbit coupling, *Phys. Rev. B* **89**, 020505 (2014).
- [7] M. Sato and S. Fujimoto, Topological phases of noncentrosymmetric superconductors: Edge states, Majorana fermions, and non-Abelian statistics, *Phys. Rev. B* **79**, 094504 (2009).
- [8] Y. Tanaka, Y. Mizuno, T. Yokoyama, K. Yada, and M. Sato, Anomalous Andreev bound state in noncentrosymmetric superconductors, *Phys. Rev. Lett.* **105**, 097002 (2010).
- [9] M. Sato and Y. Ando, Topological superconductors: A review, *Rep. Prog. Phys.* **80**, 076501 (2017).
- [10] X.-L. Qi and S.-C. Zhang, Topological insulators and superconductors, *Rev. Mod. Phys.* **83**, 1057 (2011).
- [11] C. Kallin and J. Berlinsky, Chiral superconductors, *Rep. Prog. Phys.* **79**, 054502 (2016).
- [12] E. Bauer, G. Hilscher, H. Michor, C. Paul, E. W. Scheidt, A. Gribanov, Y. Seropegin, H. Noël, M. Sigrist, and P. Rogl, Heavy fermion superconductivity and magnetic order in noncentrosymmetric  $\text{CePt}_3\text{Si}$ , *Phys. Rev. Lett.* **92**, 027003 (2004).
- [13] Y. Muro, D. Eom, N. Takeda, and M. Ishikawa, Contrasting Kondo-lattice behavior in  $\text{CeTSi}_3$  and  $\text{CeTGe}_3$  ( $T = \text{Rh}$  and  $\text{Ir}$ ), *J. Phys. Soc. Jpn* **67**, 3601 (1998).
- [14] A. D. Hillier, J. Quintanilla, and R. Cywinski, Evidence for time-reversal symmetry breaking in the noncentrosymmetric superconductor  $\text{LaNiC}_2$ , *Phys. Rev. Lett.* **102**, 117007 (2009).
- [15] J. A. T. Barker, D. Singh, A. Thamizhavel, A. D. Hillier, M. R. Lees, G. Balakrishnan, D. M. Paul, and R. P. Singh, Unconventional superconductivity in  $\text{La}_7\text{Ir}_3$  revealed by muon spin relaxation: Introducing a new family of noncentrosymmetric superconductor that breaks time-reversal symmetry, *Phys. Rev. Lett.* **115**, 267001 (2015).
- [16] T. Shang, M. Smidman, A. Wang, L.-J. Chang, C. Baines, M. K. Lee, Z. Y. Nie, G. M. Pang, W. Xie, W. B. Jiang, M. Shi, M. Medarde, T. Shiroka, and H. Q. Yuan, Simultaneous nodal superconductivity and time-reversal symmetry breaking in the noncentrosymmetric superconductor  $\text{CaPtAs}$ , *Phys. Rev. Lett.* **124**, 207001 (2020).
- [17] R. P. Singh, A. D. Hillier, B. Mazidian, J. Quintanilla, J. F. Annett, D. M. Paul, G. Balakrishnan, and M. R. Lees, Detection of time-reversal symmetry breaking in the noncentrosymmetric superconductor  $\text{Re}_6\text{Zr}$  using muon-spin spectroscopy, *Phys. Rev. Lett.* **112**, 107002 (2014).
- [18] D. Singh, J. A. T. Barker, A. Thamizhavel, D. M. Paul, A. D. Hillier, and R. P. Singh, Time-reversal symmetry breaking in the noncentrosymmetric superconductor  $\text{Re}_6\text{Hf}$ : Further evidence for unconventional behavior in the  $\alpha$ -Mn family of materials, *Phys. Rev. B* **96**, 180501 (2017).
- [19] T. Shang, G. M. Pang, C. Baines, W. B. Jiang, W. Xie, A. Wang, M. Medarde, E. Pomjakushina, M. Shi, J. Mesot, H. Q. Yuan, and T. Shiroka, Nodeless superconductivity and time-reversal symmetry breaking in the noncentrosymmetric superconductor  $\text{Re}_{24}\text{Ti}_5$ , *Phys. Rev. B* **97**, 020502 (2018).
- [20] T. Shang, M. Smidman, S. K. Ghosh, C. Baines, L. J. Chang, D. J. Gawryluk, J. A. T. Barker, R. P. Singh, D. M. Paul, G. Balakrishnan, E. Pomjakushina, M. Shi, M. Medarde, A. D. Hillier, H. Q. Yuan, J. Quintanilla, J. Mesot, and T. Shiroka, Time-reversal symmetry breaking in Re-based superconductors, *Phys. Rev. Lett.* **121**, 257002 (2018).
- [21] D. Singh, M. S. Scheurer, A. D. Hillier, D. T. Adroja, and R. P. Singh, Time-reversal-symmetry breaking and unconventional pairing in the noncentrosymmetric superconductor  $\text{La}_7\text{Rh}_3$ , *Phys. Rev. B* **102**, 134511 (2020).
- [22] T. Shang, S. K. Ghosh, J. Z. Zhao, L.-J. Chang, C. Baines, M. K. Lee, D. J. Gawryluk, M. Shi, M. Medarde, J. Quintanilla, and T. Shiroka, Time-reversal symmetry breaking in the noncentrosymmetric  $\text{Zr}_3\text{Ir}$  superconductor, *Phys. Rev. B* **102**, 020503 (2020).
- [23] A. A. Aczel, T. J. Williams, T. Goko, J. P. Carlo, W. Yu, Y. J. Uemura, T. Klimczuk, J. D. Thompson, R. J. Cava, and G. M. Luke, Muon spin rotation/relaxation measurements of the noncentrosymmetric superconductor  $\text{Mg}_{10}\text{Ir}_{19}\text{B}_{16}$ , *Phys. Rev. B* **82**, 024520 (2010).
- [24] D. Singh, J. A. T. Barker, A. Thamizhavel, A. D. Hillier, D. M. Paul, and R. P. Singh, Superconducting properties and  $\mu\text{SR}$  study of the noncentrosymmetric superconductor  $\text{Nb}_{0.5}\text{Os}_{0.5}$ , *J. Phys.: Condens. Matter* **30**, 075601 (2018).
- [25] P. K. Biswas, A. D. Hillier, M. R. Lees, and D. M. Paul, Comparative study of the centrosymmetric and noncentrosymmetric superconducting phases of  $\text{Re}_3\text{W}$  using muon spin spectroscopy and heat capacity measurements, *Phys. Rev. B* **85**, 134505 (2012).
- [26] T. Shang, D. J. Gawryluk, J. A. T. Vezhzhak, E. Pomjakushina,

- M. Shi, M. Medarde, J. Mesot, and T. Shiroka, Structure and superconductivity in the binary  $\text{Re}_{1-x}\text{Mo}_x$  alloys, *Phys. Rev. Materials* **3**, 024801 (2019).
- [27] T. Shang, C. Baines, L.-J. Chang, D. J. Gawryluk, E. Pomjakushina, M. Shi, M. Medarde, and T. Shiroka,  $\text{Re}_{1-x}\text{Mo}_x$  as an ideal test case of time-reversal symmetry breaking in unconventional superconductors, *npj Quantum Mater.* **5**, 76 (2020).
- [28] A. Amato, Heavy-fermion systems studied by  $\mu\text{SR}$  technique, *Rev. Mod. Phys.* **69**, 1119 (1997).
- [29] S. J. Blundell, Spin-polarized muons in condensed matter physics, *Contemp. Physics* **40**, 175 (1999).
- [30] J. H. Brewer, Muon spin rotation/relaxation/resonance, in *digital Encyclopedia of Applied Physics*, edited by G. L. Trigg (Wiley-VCH, Weinheim, 2003) p. eap258.
- [31] A. Yaouanc and P. D. de Réotier, *Muon Spin Rotation, Relaxation, and Resonance: Applications to Condensed Matter* (Oxford University Press, Oxford, 2011).
- [32] J. E. Sonier, J. H. Brewer, and R. F. Kiefl,  $\mu\text{SR}$  studies of the vortex state in type-II superconductors, *Rev. Mod. Phys.* **72**, 769 (2000).
- [33] W. Barford and J. M. F. Gunn, The theory of the measurement of the London penetration depth in uniaxial type II superconductors by muon spin rotation, *Physica C* **156**, 515 (1988).
- [34] E. H. Brandt, Properties of the ideal Ginzburg-Landau vortex lattice, *Phys. Rev. B* **68**, 054506 (2003).
- [35] A. Maisuradze, R. Khasanov, A. Shengelaya, and H. Keller, Comparison of different methods for analyzing  $\mu\text{SR}$  line shapes in the vortex state of type-II superconductors, *J. Phys.: Condens. Matter* **21**, 075701 (2009), and references therein.
- [36] M. Tinkham, *Introduction to Superconductivity*, 2nd ed. (Dover Publications, Mineola, NY, 1996).
- [37] A. Carrington and F. Manzano, Magnetic penetration depth of  $\text{MgB}_2$ , *Physica C* **385**, 205 (2003).
- [38] R. Kubo and T. Toyabe, A stochastic model for low-field resonance and relaxation, in *Magnetic Resonance and Relaxation. Proceedings of the XIVth Colloque Ampère*, edited by R. Blinc (North-Holland, Amsterdam, 1967) pp. 810–823.
- [39] T. B. Massalski, H. Okamoto, L. Kacprzak, and P. R. Subramanian, *Binary alloy phase diagrams*, 2nd ed. (ASM International, Materials Park, OH, 1996).
- [40] B. W. Roberts, Survey of superconductive materials and critical evaluation of selected properties, *J. Phys. Chem. Ref. Data* **5**, 581 (1976).
- [41] K. Cenzual, E. Parthé, and R. M. Waterstrat,  $\text{Zr}_{21}\text{Re}_{25}$ , a new rhombohedral structure type containing 12Å-thick infinite  $\text{MgZn}_2$  (Laves)-type columns, *Acta Cryst. C* **42**, 261 (1986).
- [42] J. L. Murray, The Re-Ti (rhenium-titanium) system, *J. Phase Equilib.* **2**, 462 (1982).
- [43] T. V. Philip and P. A. Beck, CsCl-type ordered structures in binary alloys of transition elements, *JOM-J. Min. Met. Mat. S.* **9**, 1269 (1957).
- [44] D. Singh, K. P. Sajilesh, J. A. T. Barker, D. M. Paul, A. D. Hillier, and R. P. Singh, Time reversal symmetry breaking in noncentrosymmetric superconductor  $\text{Re}_6\text{Ti}$ , *Phys. Rev. B* **97**, 100505 (2018).
- [45] J. Jorda and J. Muller, The vanadium-rhenium system: Phase diagram and superconductivity, *J. Less-Common Met.* **119**, 337 (1986).
- [46] V. N. Eremenko and T. Velikanova, Intrusion phases based on metallides in ternary systems of transition metals with carbon, *Sov. Prog. Chem.* **56**, 21 (1990).
- [47] K. Matano, R. Yatagai, S. Maeda, and G.-q. Zheng, Full-gap superconductivity in noncentrosymmetric  $\text{Re}_6\text{Zr}$ ,  $\text{Re}_{27}\text{Zr}_5$ , and  $\text{Re}_{24}\text{Zr}_5$ , *Phys. Rev. B* **94**, 214513 (2016).
- [48] A. L. Giorgi and E. G. Szklarz, Superconductivity and lattice parameters of the dirhenides and ditechneides of thorium, hafnium and zirconium, *J. Less-Common Met.* **22**, 246 (1970).
- [49] C. Cirillo, R. Fittipaldi, M. Smidman, G. Carapella, C. Attanasio, A. Vecchione, R. P. Singh, M. R. Lees, G. Balakrishnan, and M. Cuoco, Evidence of double-gap superconductivity in noncentrosymmetric  $\text{Nb}_{0.18}\text{Re}_{0.82}$  single crystals, *Phys. Rev. B* **91**, 134508 (2015).
- [50] J. Chen, L. Jiao, J. L. Zhang, Y. Chen, L. Yang, M. Nicklas, F. Steglich, and H. Q. Yuan, BCS-like superconductivity in the noncentrosymmetric compounds  $\text{Nb}_x\text{Re}_{1-x}$  ( $0.13 \leq x \leq 0.38$ ), *Phys. Rev. B* **88**, 144510 (2013).
- [51] A. B. Karki, Y. M. Xiong, N. Haldolaarachchige, S. Stadler, I. Vekhter, P. W. Adams, D. P. Young, W. A. Phelan, and J. Y. Chan, Physical properties of the noncentrosymmetric superconductor  $\text{Nb}_{0.18}\text{Re}_{0.82}$ , *Phys. Rev. B* **83**, 144525 (2011).
- [52] C. S. Lue, T. H. Su, H. F. Liu, and B.-L. Young, Evidence for s-wave superconductivity in noncentrosymmetric  $\text{Re}_{24}\text{Nb}_5$  from  $^{93}\text{Nb}$  NMR measurements, *Phys. Rev. B* **84**, 052509 (2011).
- [53] B. Chen, Y. Guo, H. Wang, Q. Su, Q. Mao, J. Du, Y. Zhou, J. Yang, and M. Fang, Superconductivity in the noncentrosymmetric compound  $\text{Re}_6\text{Hf}$ , *Phys. Rev. B* **94**, 024518 (2016).
- [54] D. Singh, A. D. Hillier, A. Thamizhavel, and R. P. Singh, Superconducting properties of the noncentrosymmetric superconductor  $\text{Re}_6\text{Hf}$ , *Phys. Rev. B* **96**, 064521 (2017).
- [55] J. A. T. Barker, B. D. Breen, R. Hanson, A. D. Hillier, M. R. Lees, G. Balakrishnan, D. M. Paul, and R. P. Singh, Superconducting and normal-state properties of the noncentrosymmetric superconductor  $\text{Re}_3\text{Ta}$ , *Phys. Rev. B* **98**, 104506 (2018), and references therein.
- [56] Arushi, D. Singh, P. K. Biswas, A. D. Hillier, and R. P. Singh, Unconventional superconducting properties of noncentrosymmetric  $\text{Re}_{5.5}\text{Ta}$ , *Phys. Rev. B* **101**, 144508 (2020).
- [57] T. Mamiya, K. Nomura, and Y. Masuda, Superconductivity of tantalum-rhenium alloys, *J. Phys. Soc. Jpn.* **28**, 380 (1970).
- [58] P. K. Biswas, M. R. Lees, A. D. Hillier, R. I. Smith, W. G. Marshall, and D. M. Paul, Structure and superconductivity of two different phases of  $\text{Re}_3\text{W}$ , *Phys. Rev. B* **84**, 184529 (2011).
- [59] N. Kimura, K. Ito, H. Aoki, S. Uji, and T. Terashima, Extremely high upper critical magnetic field of the noncentrosymmetric heavy fermion superconductor  $\text{CeRhSi}_3$ , *Phys. Rev. Lett.* **98**, 197001 (2007).
- [60] I. Sugitani, Y. Okuda, H. Shishido, T. Yamada, A. Thamizhavel, E. Yamamoto, T. D. Matsuda, Y. Haga, T. Takeuchi, R. Settai, and Y. Onuki, Pressure-induced heavy-fermion superconductivity in antiferromagnet  $\text{CeIrSi}_3$  without inversion symmetry, *J. Phys. Soc. Jpn.* **75**, 043703 (2006).
- [61] E. M. Carnicom, W. Xie, T. Klimczuk, J. J. Lin, K. Górnicka, Z. Sobczak, N. P. Ong, and R. J. Cava,  $\text{TaRh}_2\text{B}_2$  and  $\text{NbRh}_2\text{B}_2$ : Superconductors with a chiral noncentrosymmetric crystal structure, *Sci. Adv.* **4**, eaar7969 (2018).
- [62] D. Singh, K. P. Sajilesh, S. Marik, A. D. Hillier, and R. P. Singh, Superconducting and normal state properties of the noncentrosymmetric superconductor  $\text{NbOs}_2$  investigated by muon spin relaxation and rotation, *Phys. Rev. B* **99**, 014516 (2019).
- [63] D. Singh, K. P. Sajilesh, S. Marik, A. D. Hillier, and R. P. Singh, Superconducting properties of the noncentrosymmetric superconductor  $\text{TaOs}$ , *Supercond. Sci. Technol.* **30**, 125003 (2017).
- [64] D. A. Mayoh, J. A. T. Barker, R. P. Singh, G. Balakrishnan, D. M. Paul, and M. R. Lees, Superconducting and normal-state properties of the noncentrosymmetric superconductor  $\text{Re}_6\text{Zr}$ , *Phys. Rev. B* **96**, 064521 (2017).
- [65] G. M. Pang, Z. Y. Nie, A. Wang, D. Singh, W. Xie, W. B. Jiang, Y. Chen, R. P. Singh, M. Smidman, and H. Q. Yuan, Fully gapped superconductivity in single crystals of noncentrosymmetric  $\text{Re}_6\text{Zr}$  with broken time-reversal symmetry, *Phys. Rev. B* **97**, 224506 (2018).
- [66] P. Parab, D. Singh, S. Haram, R. P. Singh, and S. Bose, Point contact Andreev reflection studies of a non-centro symmetric superconductor  $\text{Re}_6\text{Zr}$ , *Sci. Rep.* **9**, 2498 (2019).
- [67] H. Q. Yuan, D. F. Agterberg, N. Hayashi, P. Badica, D. Van-

- dervelde, K. Togano, M. Sigrist, and M. B. Salamon, *s*-wave spin-triplet order in superconductors without inversion symmetry:  $\text{Li}_2\text{Pd}_3\text{B}$  and  $\text{Li}_2\text{Pt}_3\text{B}$ , *Phys. Rev. Lett.* **97**, 017006 (2006).
- [68] M. Nishiyama, Y. Inada, and G.-q. Zheng, Spin triplet superconducting state due to broken inversion symmetry in  $\text{Li}_2\text{Pt}_3\text{B}$ , *Phys. Rev. Lett.* **98**, 047002 (2007).
- [69] W. Xie, P. R. Zhang, B. Shen, W. B. Jiang, G. M. Pang, T. Shang, C. Gao, M. Smidman, and H. Q. Yuan,  $\text{CaPtAs}$ : a new non-centrosymmetric superconductor, *Sci. China-Phys. Mech. Astron.* **63**, 237412 (2020).
- [70] K. V. Samokhin, E. S. Zijlstra, and S. K. Bose,  $\text{CePt}_3\text{Si}$ : An unconventional superconductor without inversion center, *Phys. Rev. B* **69**, 094514 (2004).
- [71] D. V. Suetin and A. L. Ivanovskii, Comparative study of electronic structure of cubic and hexagonal phases of  $\text{Re}_3\text{W}$  as non-centrosymmetric and centrosymmetric low- $T_c$  superconductors, *Intermetallics* **34**, 101 (2013).
- [72] M. J. Winiarski, Electronic structure of non-centrosymmetric superconductors  $\text{Re}_{24}(\text{Nb};\text{Ti})_5$  by *ab initio* calculations, *J. Alloys. Compd.* **616**, 1 (2014).
- [73] A. K. Mojammel, A. B. Karki, T. Samanta, D. Browne, S. Stadler, I. Vekhter, A. Pandey, P. W. Adams, D. P. Young, S. Teknowijoyo, K. Cho, R. Prozorov, and D. E. Graf, Complex superconductivity in the noncentrosymmetric compound  $\text{Re}_6\text{Zr}$ , *Phys. Rev. B* **94**, 144515 (2016).
- [74] T. Shang, J. Philippe, J. A. T. Verezhak, Z. Guguchia, J. Z. Zhao, L.-J. Chang, M. K. Lee, D. J. Gawryluk, E. Pomjakushina, M. Shi, M. Medarde, H.-R. Ott, and T. Shiroka, Nodeless superconductivity and preserved time-reversal symmetry in the noncentrosymmetric  $\text{Mo}_3\text{P}$  superconductor, *Phys. Rev. B* **99**, 184513 (2019).
- [75] S. Yip, Noncentrosymmetric superconductors, *Annu. Rev. Condens. Matter Phys.* **5**, 15 (2014).
- [76] G. M. Luke, A. Keren, L. P. Le, W. D. Wu, Y. J. Uemura, D. A. Bonn, L. Taillefer, and J. D. Garrett, Muon spin relaxation in  $\text{UPt}_3$ , *Phys. Rev. Lett.* **71**, 1466 (1993).
- [77] G. M. Luke, Y. Fudamoto, K. M. Kojima, M. I. Larkin, J. Merrin, B. Nachumi, Y. J. Uemura, Y. Maeno, Z. Q. Mao, Y. Mori, H. Nakamura, and M. Sigrist, Time-reversal symmetry-breaking superconductivity in  $\text{Sr}_2\text{RuO}_4$ , *Nature* **394**, 558 (1998).
- [78] J. Xia, Y. Maeno, P. T. Beyersdorf, M. M. Fejer, and A. Kapitulnik, High resolution polar Kerr effect measurements of  $\text{Sr}_2\text{RuO}_4$ : Evidence for broken time-reversal symmetry in the superconducting state, *Phys. Rev. Lett.* **97**, 167002 (2006).
- [79] Y. Aoki, A. Tsuchiya, T. Kanayama, S. R. Saha, H. Sugawara, H. Sato, W. Higemoto, A. Koda, K. Ohishi, K. Nishiyama, and R. Kadono, Time-reversal symmetry-breaking superconductivity in heavy-fermion  $\text{PrOs}_4\text{Sb}_{12}$  detected by muon-spin relaxation, *Phys. Rev. Lett.* **91**, 067003 (2003).
- [80] E. R. Schemm, W. J. Gannon, C. M. Wishne, W. P. Halperin, and A. Kapitulnik, Observation of broken time-reversal symmetry in the heavy-fermion superconductor  $\text{UPt}_3$ , *Science* **345**, 190 (2014).
- [81] A. D. Hillier, J. Quintanilla, B. Mazidian, J. F. Annett, and R. Cywinski, Nonunitary triplet pairing in the centrosymmetric superconductor  $\text{LaNiGa}_2$ , *Phys. Rev. Lett.* **109**, 097001 (2012).
- [82] S. Ran, C. Eckberg, Q.-P. Ding, Y. Furukawa, T. Metz, S. R. Saha, I.-L. Liu, M. Zic, H. Kim, J. Paglione, and N. P. Butch, Nearly ferromagnetic spin-triplet superconductivity, *Science* **365**, 684 (2019).
- [83] K. Ishida, H. Mukuda, Y. Kitaoka, K. Asayama, Z. Q. Mao, Y. Mori, and Y. Maeno, Spin-triplet superconductivity in  $\text{Sr}_2\text{RuO}_4$  identified by  $^{17}\text{O}$  Knight shift, *Nature* **396**, 658 (1998).
- [84] H. Tou, Y. Kitaoka, K. Ishida, K. Asayama, N. Kimura, Y. Ōnuki, E. Yamamoto, Y. Haga, and K. Maezawa, Nonunitary spin-triplet superconductivity in  $\text{UPt}_3$ : Evidence from  $^{195}\text{Pt}$  Knight shift study, *Phys. Rev. Lett.* **80**, 3129 (1998).
- [85] A. P. Mackenzie and Y. Maeno, The superconductivity of  $\text{Sr}_2\text{RuO}_4$  and the physics of spin-triplet pairing, *Rev. Mod. Phys.* **75**, 657 (2003), and references therein.
- [86] R. Joynt and L. Taillefer, The superconducting phases of  $\text{UPt}_3$ , *Rev. Mod. Phys.* **74**, 235 (2002), and references therein.
- [87] W.-C. Lee, S.-C. Zhang, and C. Wu, Pairing state with a time-reversal symmetry breaking in FeAs-based superconductors, *Phys. Rev. Lett.* **102**, 217002 (2009).
- [88] S. Sharma, Arushi, K. Motla, J. Beare, M. Nugent, M. Pula, T. J. Munsie, A. D. Hillier, R. P. Singh, and G. M. Luke, Fully gapped superconductivity in centrosymmetric and noncentrosymmetric Re-B compounds probed with  $\mu\text{SR}$ , *Phys. Rev. B* **103**, 104507 (2021).
- [89] T. Shang, A. Amon, D. Kasinathan, W. Xie, M. Bobnar, Y. Chen, A. Wang, M. Shi, M. Medarde, H. Q. Yuan, and T. Shiroka, Enhanced  $T_c$  and multiband superconductivity in the fully-gapped  $\text{ReBe}_{22}$  superconductor, *New J. Phys.* **21**, 073034 (2019).
- [90] Z. F. Weng, J. L. Zhang, M. Smidman, T. Shang, J. Quintanilla, J. F. Annett, M. Nicklas, G. M. Pang, L. Jiao, W. B. Jiang, Y. Chen, F. Steglich, and H. Q. Yuan, Two-gap superconductivity in  $\text{LaNiGa}_2$  with nonunitary triplet pairing and even parity gap symmetry, *Phys. Rev. Lett.* **117**, 027001 (2016).
- [91] J. Quintanilla, A. D. Hillier, J. F. Annett, and R. Cywinski, Relativistic analysis of the pairing symmetry of the noncentrosymmetric superconductor  $\text{LaNiC}_2$ , *Phys. Rev. B* **82**, 174511 (2010).
- [92] S. Yang, C. Wang, H. Sahin, H. Chen, Y. Li, S.-S. Li, A. Suslu, F. M. Peeters, Q. Liu, J. Li, and S. Tongay, Tuning the optical, magnetic, and electrical properties of  $\text{ReSe}_2$  by nanoscale strain engineering, *Nano Lett.* **15**, 1660 (2015).
- [93] V. Kochat, A. Apte, J. A. Hachtel, H. Kumazoe, A. Krishnamoorthy, S. Susarla, J. C. Idrobo, F. Shimojo, P. Vashishta, R. Kalia, A. Nakano, C. S. Tiwary, and P. M. Ajayan, Re doping in 2D transition metal dichalcogenides as a new route to tailor structural phases and induced magnetism, *Adv. Mater.* **29**, 1703754 (2017).